JOURNAL OF GEOPHYSICAL RESEARCH, VOL. 111, F04009, doi:10.1029/2006JF000467, 2006

Form drag in rivers due to small-scale natural topographic features: 1. Regular sequences

Jason W. Kean[1] and J. Dungan Smith[1]

Received 11 January 2006; revised 5 July 2006; accepted 11 August 2006; published 6 December 2006.

[1] Small-scale topographic features are commonly found on the boundaries of natural rivers, streams, and floodplains. A simple method for determining the form drag on these features is presented, and the results of this model are compared to laboratory measurements. The roughness elements are modeled as Gaussian-shaped features defined in terms of three parameters: a protrusion height, H; a streamwise length scale, σ; and a spacing between crests, λ. This shape is shown to be a good approximation to a wide variety of natural topographic bank features. The form drag on an individual roughness element embedded in a series of identical elements is determined using the drag coefficient of the individual element and a reference velocity that includes the effects of roughness elements further upstream. In addition to calculating the drag on each element, the model determines the spatially averaged total stress, skin friction stress, and roughness height of the boundary. The effects of bank roughness on patterns of velocity and boundary shear stress are determined by combining the form drag model with a channel flow model. The combined model shows that drag on small-scale topographic features substantially alters the near-bank flow field. These methods can be used to improve predictions of flow resistance in rivers and to form the basis for fully predictive (no empirically adjusted parameters) channel flow models. They also provide a foundation for calculating the near-bank boundary shear stress fields necessary for determining rates of sediment transport and lateral erosion.

Citation: Kean, J. W., and J. D. Smith (2006), Form drag in rivers due to small-scale natural topographic features: 1. Regular sequences, *J. Geophys. Res.*, *111*, F04009, doi:10.1029/2006JF000467.

1. Introduction

[2] The beds and banks of natural rivers and streams, and the surfaces of floodplains, often are covered with a variety of small-scale topographic features. The small-scale features on the beds of rivers include bed forms, scour holes, and clusters of clasts. On the banks of rivers they consist of undulations produced by erosion and slumping of bank material and undulations associated with vegetation, such as protruding root balls and protrusions of grass sod. Flow over or past these small-scale topographic features produces form drag on them, which can substantially affect the overall flow resistance of the channel, as well as the flow and sediment transport patterns within the channel. Accurate quantitative treatment of the small-scale features is essential for determining overall and local flow resistance in fully predictive river flow models. Furthermore, understanding the complicated flow patterns as affected by the small-scale features on the beds and banks of streams and rivers is essential for calculating bed and bank erosion. For example, the roughness of the bank and that of the near-by stream bed control the boundary shear stress field in the neighborhood of the toe of a cutbank, and it is the shear stress field in this area that, in turn, controls the nature and rate of bank erosion and thus meander migration.

[3] Studies aimed at understanding the flow and boundary shear stress over small-scale topographic features in rivers have focused primarily on the flow over bed forms. One approach to this problem, taken by *Smith and McLean* [1977] in a study of flow over dunes in the Columbia River, involves partitioning the total stress on the boundary into a stress due to drag on the topographic features and a stress acting on the actual boundary, which they called skin-friction. The skin friction, which scales the near-boundary flow and controls the sediment transport, can be determined by subtracting the drag stress from the total stress on the boundary. The latter is known, for example, from the depth-slope product in an unaccelerated flow or from a flow model in a more complicated flow. In the Smith and McLean method the drag on the dune is calculated using a drag coefficient for the bed form and an appropriate reference velocity. This method was originally tested using flow measurements made in the Columbia River. A major advantage of this method is that the roughness effects of the bed forms can be readily tied to their geometric properties, such as shape, height, and spacing. More recently, methods in computational fluid dynamics (CFD) also have been used to study flow over bed topographic features, such as dunes [e.g., *Patel and Yoon*, 1995] and surface irregularities on

[1]U.S. Geological Survey, Boulder, Colorado, USA.

gravel beds [e.g., *Olsen and Stokseth*, 1995; *Lane et al.*, 2004; *Nicholas*, 2005]. The complex flow produced by rough surfaces is particularly difficult to model using available computational methods [*Patel*, 1998]. For this reason, numerical studies have only recently moved beyond modeling laboratory situations with regular, well-defined boundaries. While the use of CFD to study flow over complex natural topography shows considerable promise [e.g., *Lane et al.*, 2004], the approach remains computationally intensive and usually requires ultrahigh-resolution topographic data sets, which are difficult to obtain.

[4] Despite the importance of bank roughness in controlling bank erosion, relatively little has been done to characterize it. A common feature of natural banks, which make them difficult to model, is that their surfaces are highly irregular. The size and shape of bank features is influenced by a wide variety of environmental factors, including vegetation, soil cohesion, and flow. As a consequence, the size and spacing of adjacent features can vary considerably, usually more than the geometry of a set of dunes. In addition to this variability, the shape of bank features tends to be shorter, steeper, and more symmetric than that of dunes. These characteristics result in greater form drag relative to the dune situation and a wake that substantially affects the flow over the features further downstream.

[5] A first step toward understanding this complicated interaction was taken by *Hopson* [1999] using a series of flume experiments. These experiments measured the drag coefficients of several different Gaussian-shaped elements placed on the flume wall, as well as the drag force on an element placed within a series of identical, regularly spaced Gaussian elements on the flume wall. A Gaussian shape was chosen for the profile of the roughness elements for several reasons. This shape provided (1) a well-defined point of separation, (2) a smooth transition onto the underlying boundary of the channel, (3) a simple analytical expression, (4) a single pair of inflection points, and (5) a small set of parameters characterizing its shape so that it would be easy to apply to stream-bank irregularities. In the latter context, the Gaussian shape provided the three essential parameters for approximating a natural small-scale topographic element, namely (1) a protrusion distance, H, (2) a streamwise span (equivalent to the standard deviation, σ, in a Gaussian probability distribution), (3) and a spacing of the crests. A Gaussian curve can express a wide variety of shapes by varying the ratio of its streamwise length scale to cross-stream length scale, and, as will be shown subsequently, provides a satisfactory approximation to a wide variety of roughness elements found on the banks of rivers.

[6] The goal of this paper and a companion paper [*Kean and Smith*, 2006], which are continuations of the work of *Hopson* [1999], is to develop models to calculate the flow and boundary shear stress fields over a boundary that is characteristic of natural river banks. These papers are only concerned with the flow effects of topographic features; treatment of the flow effects of other roughness elements commonly found on stream banks, such as the stems and branches of woody vegetation, which are better modeled as circular cylindrical elements, can be found elsewhere [e.g., *Kean and Smith*, 2004; *Griffin et al.*, 2005]. Using an approach similar to the one developed by *Smith and McLean* [1977] for dunes, a model for low Froude number flow ($Fr < 1$) past a regular sequence of two-dimensional bank elements is developed in this paper and the results are compared to data from the *Hopson* [1999] experiment. Owing to the close spacing and relatively blunt geometry of typical bank roughness elements, the new model places a greater emphasis on characterizing the velocity in the wake region behind Gaussian-shaped roughness elements than is required for the dune problem. The new model is then used together with the flow model of *Kean and Smith* [2004] to investigate the effects of bank roughness on patterns of velocity and boundary shear stress in a channel. A generalization of the model presented herein that accommodates irregular sequences of topographic elements is described in the companion paper [*Kean and Smith*, 2006]. Although the focus of the models discussed in these two papers is on bank topographic roughness, the modeling approach is valid for any boundary on which the small-scale topographic features can be approximated by Gaussian-shaped elements. Specifically, it can be used for floodplains, riverbeds, and the sea floor, as well as river banks.

2. Natural Topographic Bank Features

[7] Three streamwise example profiles of bank surface topography in channels near U.S Geological Survey (USGS) streamflow gauging stations are shown in Figure 1. These profiles were measured as part of an ongoing effort by the authors to develop and test a fluid mechanically based method to calculate stage-discharge relations (theoretical rating curves) for natural channels. This new method of stream gauging determines the flow resistance in the channel from basic geometric measurements of the roughness elements in the channel, including bed material, woody vegetation, and small-scale topographic features such as those shown in the Figure 1. Quantifying the resistance of the small-scale bank topographic features is essential for determining accurate theoretical rating curves for each of these three sites, because the channels are narrow relative to their depth. The flow resistance associated with the first example of bank topography shown in Figure 1 (from Lost Creek) will be discussed later in this paper. That associated with each of the second two examples (from Rock Creek and Whitewater River) along with the resulting theoretical rating curves is discussed by *Kean and Smith* [2005].

[8] The measurements for the first two examples (A, B) were made by placing a 9-m long straight edge along the bank parallel to the flow direction and then recording the distance normal to the bank surface at 5-cm intervals. The measurements in the third example (C) were made using a total station. In all cases, long-wavelength oscillations, which are 5 to 10 topographic features in length and correspond to the general shape of the channel, have been removed from the data [see *Kean and Smith*, 2005]. These long-wavelength undulations tend to produce a negligible contribution to the flow resistance in the channel.

[9] The topographic features shown in these three examples are essentially two-dimensional in shape; i.e., there is little change in the profiles with elevation above the bed. In some channels streamwise profiles of bank topography vary

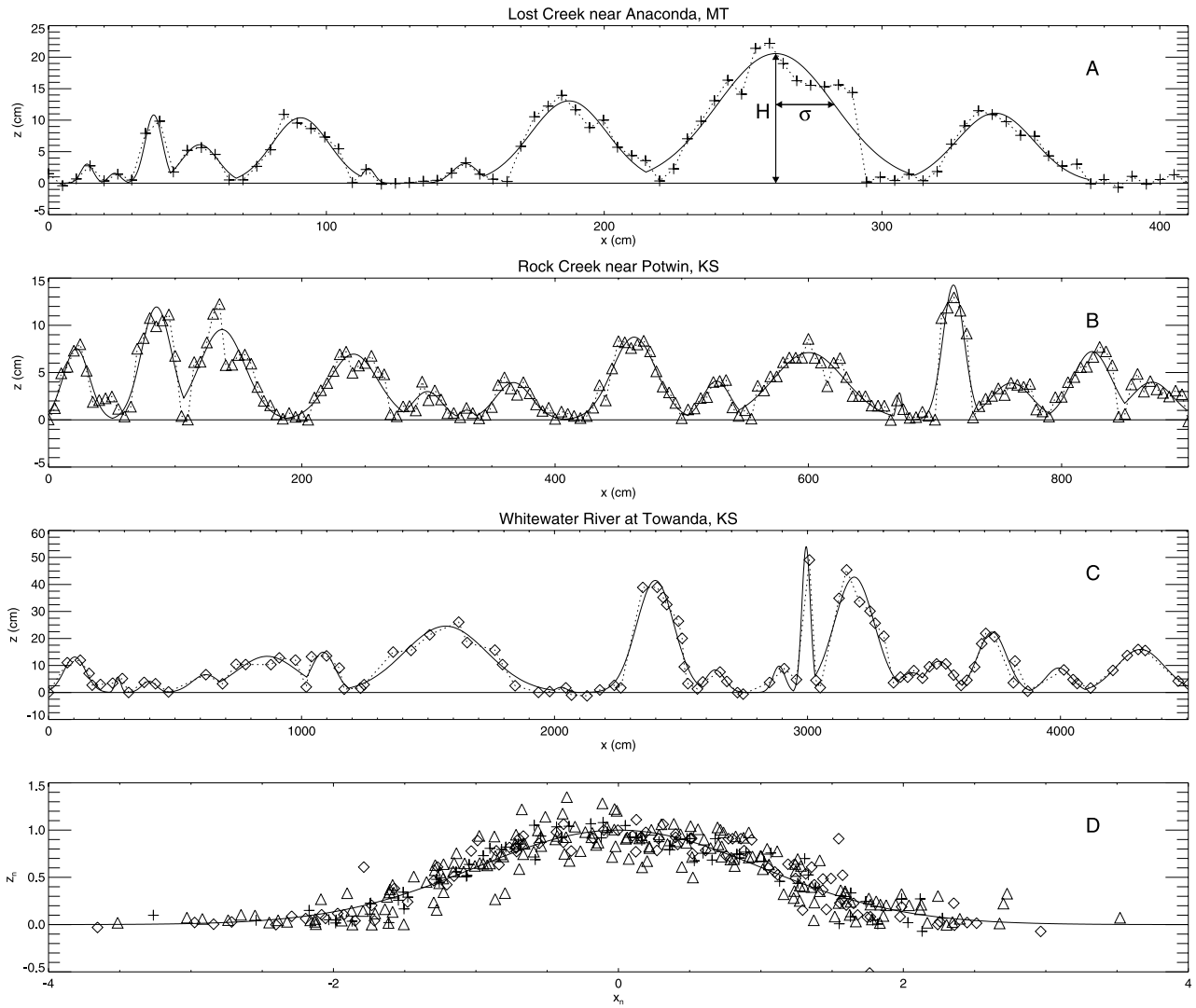

Figure 1. Measurements of bank topographic profiles near USGS streamflow gauging stations (a) 12323840, Lost Creek near Anaconda, Montana, (b) 07146995, Rock Creek near Potwin, Kansas, and (c) 07147070, Whitewater River at Towanda, Kansas. A best fit Gaussian curve is shown for each topographic feature. (d) Standard normalized Gaussian curve plotted together with measurements normalized by H and σ and the streamwise position of the center of each feature.

gradually with elevation above the bed. In these cases, such variation usually follows a trend of decreasing protrusion heights from the top of the bank to the bed. In addition to the gradual variation with elevation, the mean geometric properties of bank topography that control roughness also can change in the streamwise direction. Thus, in order to characterize bank roughness fully within a reach of interest, many profiles, such as those shown in Figure 1, are required. These profiles should be made at different elevations along the bank, as well as at different streamwise positions in the channel.

[10] The three examples of bank roughness shown in Figure 1 are taken from channels spanning a wide range in size and bankfull discharge (Table 1). The banks in each case also are composed of different materials and shaped by different mechanisms. Lost Creek, the smallest and narrowest channel, has very steep banks composed of fine grained alluvium and closely spaced willows. The bank cohesion provided by willow roots supports bank protrusions that are as large as 5% of the width of the channel. The banks of Rock Creek are vegetated less densely than Lost Creek and are composed of a mixture of fine-grained sediment and limestone clasts. These banks and their protrusions tend to be less steep than at Lost Creek. The bank topography of the Whitewater River at Towanda, the largest channel, is controlled primarily by local slumping of the fine-grained bank material. The small-scale topographic features at that site tend to be larger and broader than in the two smaller channels. Despite substantial differences in channel size and bank characteristics, the shape of most of the individual topographic elements is well approximated using features with a Gaussian cross section. The deviations of the measured topography from the Gaussian fits can be treated as a smaller scale of roughness superimposed on the

Table 1. Summary of Channel Characteristics for the Channels in Figure 1

	Drainage Area, km^2	Bankfull Width, m	Bankfull Depth, m	Bankfull Discharge, m^3/s
Lost Creek, MT	68	4.5	1	5
Rock Creek, KS	32	8.8	1.6	20
Whitewater River, KS	1100	33	5.5	170

Gaussian shapes. Methods to estimate the magnitude of this smaller scale of roughness are described by *Kean and Smith* [2005, 2006].

3. Model for a Regular Sequence of Topographic Elements

[11] Following the approach of *Smith and McLean* [1977], the total shear stress on the average boundary of a channel, τ_T, can be partitioned into two components: an average shear stress on the actual surface, τ_{SF} (called "skin friction" by *Smith and McLean* [1977]), and a shear stress on the average channel boundary due to form drag on the boundary irregularities, τ_D. This partition of shear stress can be written as

$$\tau_T = \tau_{SF} + \tau_D \tag{1}$$

The "skin friction" is the result of fluid stresses acting on the boundary that arise from there being a no-slip condition at the wall. The "drag stress" is the result of pressure forces acting on the surfaces of elements which protrude into the flow. Flow past a protruding topographic element creates a pressure differential on the element between its upstream and downstream sides that is highly dependent on its shape (or form). This pressure differential produces a force (or form drag) on the element. The drag stress is the form drag on the element divided by the area of boundary over which the drag force is applied, which depends on the spacings of the topographic elements comprising the boundary.

[12] Because of the high Reynolds number of river flows and the relatively blunt shape of bank topographic elements, the drag stress is usually the dominant shear stress transmitted to the boundary. Owing to this dominance, the drag stress must be carefully incorporated into any accurate near-boundary flow model. The drag (F) on an individual element is expressed by the equation

$$F = \frac{1}{2}\rho C_D H B u_{ref}^2 \tag{2}$$

where ρ is the density of water, H is the protrusion height of the element, B is the length of the direction perpendicular to the x and z axis defined in Figure 2, u_{ref} is an appropriately determined reference velocity, and C_D is the empirically determined drag coefficient of the element. For high Reynolds number flows, such as occurred in the experiment and as occur in rivers, C_D is a function of the shape of the object and is nearly independent of the Reynolds number. Given H, B, and C_D for a topographic element, (2) can be used to determine the drag force on an object in any flow scenario, provided that the appropriate u_{ref} is employed.

[13] The square of the reference velocity is defined to be the average of the square of the velocity that would be present if the element were removed from the flow. In the case of a single element placed in a streamwise uniform flow, this average is taken across the elements's cross-sectional area perpendicular to the flow (H B). When the near-boundary flow is evolving in the streamwise direction, such as for an element embedded in a series of regularly spaced elements on a boundary, a robust estimate of u_{ref} can be made by averaging the square of the velocity over the volume the element occupies. The plan view of the averaging domain for u_{ref} is depicted by the dashed Gaussian curve in Figure 2. The model presented in this paper provides a means by which u_{ref} can be determined for flow over a sequence of elements on the bank using the geometry, spacing, and C_D of the elements, as well as, either a specified far-field velocity away from the bank or the specified total shear stress on the boundary. Through the process of calculating u_{ref}, the form drag on the boundary, the total roughness height of the boundary due to skin friction plus form drag, z_{oT}, and the spatially averaged velocity field from the wall of the channel to the far-field also are determined.

[14] For each topographic element in a long train of regularly spaced similar topographic elements, the reference velocity is primarily controlled by the wake of the upstream element. This wake, in turn, is affected by the flow above it, which is created by the resistance of the roughness elements further upstream. In addition to the wake, u_{ref} is affected by

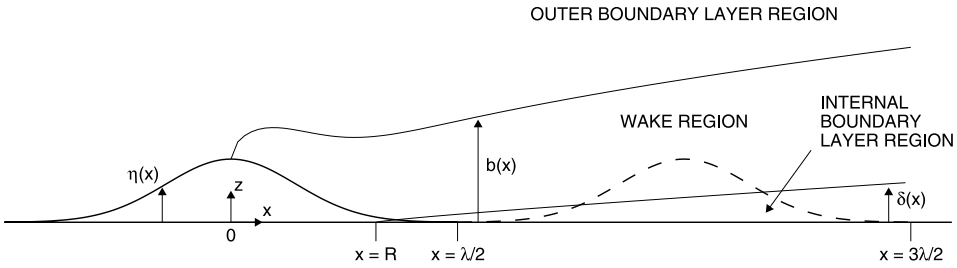

Figure 2. Diagram of the plan view geometry of topographic roughness elements and the internal boundary layer, wake, and outer regions of flow. The dashed line of the downstream element indicates that it is removed from the flow, and u_{ref}^2 for this element is the average squared velocity over this area. The unit "cell" from $\lambda/2$ to $3\lambda/2$ is the length over which the stresses are averaged.

a growing internal boundary layer on the wall that begins at the reattachment point of the separation zone on the upstream form. The internal boundary layer is scaled by the wake above it. Thus u_{ref} is affected by three interdependent regions each having turbulent processes which scale differently. They are: an internal boundary layer region, a wake region, and an outer boundary layer region (Figure 2). In order to calculate u_{ref}, the velocity field of each region must be determined.

[15] In keeping with the approach used by *Smith and McLean* [1977] and *McLean and Smith* [1986], this model describes the velocity field in each region separately and joins the regions together using appropriate matching conditions. This approach is based on the assumption that the turbulence in each region is governed by low-order momentum balances. The alternatives to this approach are either to solve the Reynolds-averaged Navier-Stokes equations using a turbulence closure capable of describing the complicated flow regions or to perform a direct numerical simulation of the nonaveraged equations. The computational intensity of the latter method make it not well suited for describing the wide variety natural configurations that are of interest in this study. Computational fluid dynamic models following the former approach are now being used to study the flow over complex bed topography [e.g., *Lane et al.*, 2004]. While it is likely that these methods will eventually be employed successfully to address problems involving complex bank topography, simpler semianalytic approaches, such as the one presented here, are sufficient to gain the desired insight into the problem.

3.1. Three Flow Regions

[16] The lowest region of flow can be described by a growing internal boundary layer that begins at the reattachment point, R, of the separation zone of the upstream element. The accelerating flow in this region is initially laminar but quickly becomes turbulent for the flow conditions of in most rivers. Therefore, for most of the internal boundary layer, the velocity can be described by the turbulent law of the wall, which is given by the equation

$$u = \frac{u_{*IBL}}{\kappa} \ln \frac{z}{z_{oSF}} \tag{3}$$

where κ is von Karman's constant = 0.408 [*Long et al.*, 1993], z is the distance away from the boundary, z_{oSF} is the local roughness height of the boundary without the topographic elements, and u_{*IBL} is the shear velocity inside the internal boundary layer, which is equal to $\sqrt{\tau_{IBL}/\rho}$. Here τ_{IBL} is the local skin friction shear stress that would be present if the object were removed from the flow. This stress is similar but not equivalent to the actual skin friction shear stress acting on the surface of the roughness element, τ_{SF}. In addition to being affected by a growing internal boundary layer, the actual skin friction shear stress on the topographic element also is affected by pressure gradients produced from flow past the object, which cause acceleration of the fluid on the upstream side of the element and flow separation downstream from the crest. For broad, low topographic features, such as dunes, the spatial average of τ_{SF} is very close to the average of τ_{IBL}.

[17] The thickness of the internal boundary layer is estimated here using an approach suggested by *Miyake* [1965]. This approach is based on the assumption that the rate of vertical diffusion of the boundary layer is related to the local shear velocity. From this assumption, the slope of the internal boundary layer height is given by

$$\frac{d\delta}{dx} = \frac{\gamma u_{*IBL}}{u_\delta} \tag{4}$$

where δ is the boundary layer height, u_δ is velocity at the top of the boundary layer, and γ is a constant of order 1. After substituting $u\delta$ from the logarithmic profile given by (3) but evaluated at $z = \delta$ into (4), equation (4) may be integrated with the initial condition that $\delta = z_{oSF}$ at $x' = x - R$ to give an implicit expression for δ, which is

$$\frac{\delta}{x'}\left[\ln\left(\frac{\delta}{z_{oSF}}\right) - 1\right] = \gamma\kappa \tag{5}$$

where x' is the distance downstream from the beginning of the turbulent boundary layer. Using the value of 1.25 for γ, (5) has been shown by *Walmsley* [1989] to give good agreement with atmospheric measurements of internal boundary layers in wind profiles over a change in the surface roughness.

[18] The wake region above the internal boundary layer is modeled using Schlichting's far-field wake solution [*Schlichting*, 1979], which was used by *McLean and Smith* [1986] to model the wakes of dunes. The wake solution of *Schlichting and Gersten* [2000] could be used just as well. Both are similarity solutions obtained from the linearized momentum integral, which use the assumption that the velocity deficit, or difference between the velocity inside and outside the wake, is small. This assumption usually becomes valid at greater distances downstream from objects than are of interest here. It appears, however, that the wake evolves to exhibit some degree of self-similarity much before the far-field assumption becomes valid. Placing the centerline of the wake on the boundary, the Schlichting solution is given by

$$u = u_b\left[1 - g(x) f\left(\frac{z-\eta}{b}\right)\right] \tag{6}$$

where

$$g(x) = A_2\left(\frac{x + x_o}{C_D H}\right)^{-1/2} \quad \text{and} \quad f\left(\frac{z-\eta}{b}\right) = \left[1 - \left(\frac{z-\eta}{b}\right)^{3/2}\right]^2$$

In these equations, A_2 is a constant, x is the distance downstream from the center of the object producing the wake, z is the distance away from the reference level of the roughness elements, $z = \eta$ is the surface of the boundary, b is the wake thickness, C_D is the drag coefficient of the object, H is the height of the upstream object, u_b is the velocity at the top of the wake, and x_o is the virtual origin, which, in this problem, is taken to be equal to zero. In principal, the x axis should conform to the surface of the boundary containing the roughness elements; however, for simplicity, the x axis is approximated to be along the

reference level of the roughness elements as shown in Figure 2.

[19] The wake thickness is given by the equation

$$b = 2A_1 C_D H \left(\frac{x + x_o}{C_D H}\right)^{1/2} \tag{7}$$

where A_1 is a constant. The constants A_1 and A_2 are equal to $\sqrt{10}\beta$ and $\sqrt{20}/(18\beta)$, respectively, where β is an empirically determined constant that sets the eddy viscosity within the wake. Schlichting determined β to be 0.18 using velocity measurements behind a circular cylinder. Given that the centerline of the wake has been replaced by a solid boundary, it is expected that the constant for this application may differ somewhat from that determined by Schlichting, and it will be left to be determined empirically from the measurements of *Hopson* [1999]. It is important to note that parameters C_D, H, and b in (6) and (7) are tied to the element producing the wake and not the element for which the reference velocity is to be calculated. For a regular sequence, however, these parameters are the identical for each element.

[20] The internal boundary layer and wake are matched by equating the velocity at the top of the boundary layer to the velocity of the wake at z = δ. This matching condition results in a discontinuity in shear at this level, but is retained for its simplicity. The average skin friction based shear velocity for the "cell" can then be related to u_b by

$$\left\langle u_{*IBL} \right\rangle = \alpha_1 u_b \tag{8}$$

where $\langle\ \rangle$ denotes a spatial average and

$$\alpha_1 = \frac{1}{\lambda_i} \int_{x1}^{x2} \left[1 - g(x) f\left(\frac{\delta}{b}\right)\right] \left[\frac{1}{\kappa} \ln\left(\frac{z}{z_o}\right)\right]^{-1} dx \tag{9}$$

In this equation, the subscript i refers to the "cell" containing the element for which the reference velocity is needed; the subscript $i–1$ refers to the upstream "cell" containing the wake-producing element. The upper limit of integration is $x_2 = (\lambda_{i-1})/2 + \lambda_i$, where λ_i and λ_{i-1} are the widths of the current and upstream cells. The lower limit depends on whether the separation zone extends into the unit cell. If it does, $x_1 = R_{i-1}$, and if not, $x_2 = (\lambda_{\ i-1})/2$, where $R_{i\ -\ 1}$ is the position of the upstream reattachment point. In this paper, the value of R for an element is obtained from (6) as the position of zero wake velocity at the boundary, which is given by $C_D H A_2^2$.

[21] The loss of momentum from drag and skin friction on the roughness elements causes momentum to diffuse inward toward the boundary and, in an equilibrium situation, produces a logarithmic velocity profile given by

$$u = \frac{u_{*T}}{\kappa} \ln\left(\frac{z}{z_{oT}}\right) \tag{10}$$

where $u_{*T} = \sqrt{\tau_T/\rho}$ and z_{oT} is the roughness height due to skin friction plus form drag. Superimposed on this flow, are the accelerations and decelerations associated with the approximately inviscid response of the flow to the undulations of the topographic elements on the boundary [see *McLean and Smith*, 1986; *Nelson and Smith*, 1989]. This response will not be addressed in this study because it does not significantly affect the spatially averaged flow properties, which are of primary interest here.

[22] The matching condition between the wake and the outer region is specified by requiring that both the velocity and shear between the two regions be continuous. For simplicity, this condition is enforced only above the center of the element, which corresponds to the streamwise position $x = x_c = (\lambda_i + \lambda_{i-1})/2$. The velocity matching condition leads to the expression for u_b:

$$u_b = \frac{u_{*T}}{\kappa} \ln\left(\frac{z_m}{z_{oT}}\right) \left[1 - g(x_c) f\left(\frac{z_m}{b(x_c)}\right)\right]^{-1} \tag{11}$$

where z_m is the matching height. The shear matching condition leads to an implicit sixth-order polynomial expression for z_m. The only physically meaningful root of this polynomial is

$$z_m = \left[\frac{-a_2 + \sqrt{a_2^2 - 4a_1 a_3}}{2a_3}\right]^{2/3} \tag{12}$$

where

$$a_1 = 1 - g(x_c)$$

$$a_2 = -\frac{g(x_c)}{b(x_c)^{3/2}} \left[3 \ln\left(\frac{z_m}{z_{oT}}\right) - 2\right]$$

$$a_3 = \frac{g(x_c)}{b(x_c)^3} \left[3 \ln\left(\frac{z_m}{z_{oT}}\right) - 1\right]$$

Given an initial guess for z_m, (12) can be solved by iteration to find z_m. A complete match in shear is not possible for broader forms, and in these cases the real component of (12) is taken to provide the level for the closest match.

[23] Equations (3), (6), and (10) together with the matching conditions fully specify the velocity field, $u(x, y)$, that would be present if the object were removed from the flow. Having specified this field, the reference velocity for the drag equation is determined by averaging the square of this field over the space that the element occupied. For a two-dimensional flow this average is given by the equation

$$u_{ref}^2 = \frac{1}{A} \int_A u^2(x, z)\, dA \tag{13}$$

where A is the plan view area of the element. The plan view area of a Gaussian shape is given by $H\sigma\sqrt{\pi/2}\left[\mathrm{erf}(\frac{x_{dn}-x_c}{\sqrt{2}\sigma}) - \mathrm{erf}(\frac{x_{up}-x_c}{\sqrt{2}\sigma})\right]$, where x_{up} x_{dn}, and x_c are the streamwise positions of the upstream end, downstream end, and center (crest) of the element, respectively.

3.2. Closing the Solution

[24] Depending on the application, the solution is closed by specifying either the total boundary shear stress or a velocity in the outer region. For uniform flow over a sequence of topographic elements on a channel bottom or on a floodplain, the total boundary shear stress is known

from the depth-slope product. In the case of topographic elements on a bank, however, the total stress on the bank is not known a priori, because it depends on the relative roughnesses of the bank and the bed. In this situation it is more convenient to close the problem by specifying a velocity at a level in the outer region of flow. This velocity can be measured in the field or calculated using methods such as the one described by *Kean and Smith* [2004]. Because banks are the focus of this chapter, the solution will be presented in terms of a specified outer velocity; however, the steps can be easily modified to accommodate a specified boundary shear stress.

[25] In order to close the solution using either parameter, the drag on the topographic elements must be related to the properties of the outer flow through (1). Using (2), the drag stress may be expressed as

$$\tau_D = \frac{1}{2}\rho C_D \frac{H}{\lambda} u_{ref}^2 \tag{14}$$

If the average skin friction stress, τ_{SF}, is expressed in terms of $\langle \tau_{IBL} \rangle \equiv \rho \langle u_{*IBL} \rangle^2$, then the total stress on the boundary, τ_T, can be written as

$$\tau_T = \rho u_*^2 = \rho\left(\alpha_o \left\langle u_{*IBL} \right\rangle^2\right) + \frac{1}{2}\rho C_D \frac{H}{\lambda} u_{ref}^2 \tag{15}$$

where α_0 is an estimate of the ratio $u_{*SF}/\langle u_{*IBL} \rangle$, which in these calculations is taken to be 1. The overall error incurred by this approximation is minimal, because for these kinds of topographic features the skin friction stress is typically an order of magnitude less than the drag stress. Using these equations the outer flow parameters, z_{oT} and u_{*T}, can be determined by iteration. Initial guesses of z_{oT} and u_{*T} are first made that match the specified velocity at its level. Once specified, $\langle u_{*IBL} \rangle$ and u_{ref} can be determined using (8) and (13). These values can then be used to obtain improved estimates of u_{*T} and z_{oT} using (15) and (10). The procedure is repeated until the solution converges.

[26] An important feature of the solution is that the total roughness height, z_{oT}, of a regular sequence of elements is independent of the magnitude of the velocity in the outer region. This is not immediately apparent from the equations above; therefore it is shown in an Appendix. The same is true for a boundary of fixed grains in hydraulically rough flow, where z_o only depends on the geometry of the boundary. The independence z_{oT} on the flow for a regular sequence greatly simplifies the computation of the three-dimensional streamwise flow field near banks with small-scale roughness.

4. Laboratory Experiments

[27] The experiments by *Hopson* [1999] were conducted using a recirculating, variable slope flume. The walls were painted steel and the bottom was covered by 7-mm diameter gravel cemented in place. Velocity measurements used for determination of the drag coefficient of the roughness elements were made using a Prandtl tube and differential pressure transducer. Additional velocity measurements were made in the center of the flume using a partially ducted rotor current meter [*Kean*, 1998]. The

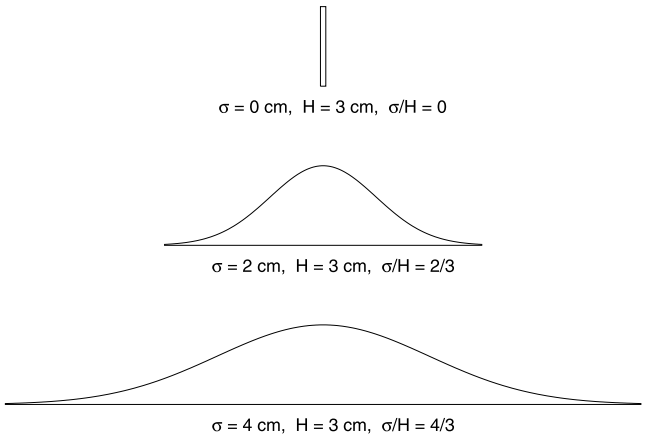

Figure 3. Shape and dimensions of three of the roughness elements used in the *Hopson* [1999] experiment. Figure 3 is drawn with the correct aspect ratio. The roughness elements extended the entire depth of the flow. The shape of the roughness elements is given by the equation $z = H \exp[(-x^2/(2\sigma^2))]$.

Gaussian-shaped roughness elements were made out of fiberglass cast from carefully built wooden molds. Deviations of the elements from the exact Gaussian shape were within 1 mm normal to the exact surface [*Hopson*, 1999]. Each type of element had the same H but different ratios of σ/H. The dimensions of three of the types are shown in Figure 3. The flat plate ($\sigma/H = 0$) provided an upper bound on the results. An intermediate Gaussian form with $\sigma/H = 1$ is not included in the present analysis because there appears to have been some error in the measurements for that element. The drag force on a roughness element was determined by measuring the strain in an aluminum bar connected to the element at one end and fixed at the other end to a rigid frame above the flume. Both the velocity and force measurements were averaged over 4 min to remove the turbulent fluctuations.

[28] Two classes of force measurements were made for each type of bank element in the *Hopson* [1999] experiment. The first class was made on a single element on the wall and was used together with velocity measurements to determine the drag coefficients for each type of roughness element. The measured drag coefficients for the three elements in Figure 3 are plotted as a function of σ/H in Figure 4. The fit to the data is given by

$$C_D = 1.79 \exp\left(-0.77 \frac{\sigma}{H}\right) \tag{16}$$

The second class of force measurements were made on an element placed in an array of ten identical elements evenly spaced along the wall as shown in Figure 5. These measurements were made to determine the effect of spacing on the drag on the elements. The force was measured on the eighth form downstream, where the flow had reached equilibrium. The spacing, λ, of the elements was varied from a minimum spacing where the elements were almost touching ($\lambda = 7\sigma$ to 6.5σ for the two Gaussian elements, and $\lambda = 4$ cm for the flat plate) to a maximum spacing of 60 cm apart. For the very close spacings of the flat plate, the

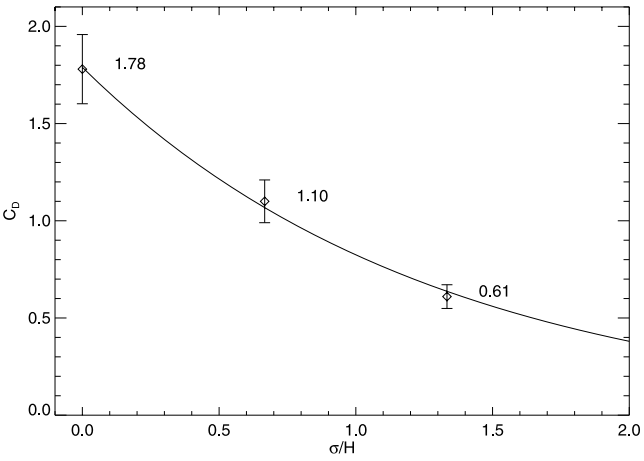

Figure 4. Measured drag coefficients of the three roughness elements shown in Figure 3. The fit to the data is given by (16). Most natural roughness elements on the banks of streams have $0.5 < \sigma/H < 2$. The error bars are ±10% of the measured value.

separation zone extended the full distance between plates. These latter cases for the flat plate are not considered in this paper.

5. Comparison to Laboratory Measurements

[29] The model is tested by comparing the measured and predicted drag forces on individual elements in a regular sequence. To account for the smooth wall of the experiment, the formulation for the flow in the internal boundary layer was changed to accommodate laminar flow near the boundary. Because of the small thickness of the internal boundary layer the reference velocity in the drag equation could be approximated by averaging only the wake velocity over the volume of the element. The empirical wake constant, β, which scales the eddy viscosity in the wake, was back-calculated from the force measurements. If the model contains the basic physics of the problem, a single value of β should provide a reasonable prediction of the measured forces for all types of forms and for a wide range of spacings. Figure 6 shows the value of β needed by the model to have perfect agreement with each of the measured values. This value will be referred to as β'. For spacings greater than $\lambda/H = 10$, β' for each type of element is nearly constant with spacing, and spans a relatively narrow range of values between 0.22 and 0.25. In the very near-field ($\lambda/H < 10$), however, β' decreases with decreasing spacings of the elements.

[30] The trends in the very near-field values of β' indicate that the drag and wake of the closely spaced elements is affected by the pressure field of the upstream element and its separation zone. These effects are not included directly in the present model. Rather than adopt a more sophisticated modeling approach for the near-field flow, the present model is retained for its simplicity, and the near-field is adjusted empirically through β' as a function of spacing. This simple approach is sufficient to provide an adequate characterization of the flow structure. The near-field fit of β is determined by regression and has the form

$$\beta = \beta_{far}\left[1 - \exp\left(-c\frac{\lambda}{H}\right)\right] \tag{17}$$

where β_{far} is the empirically determined far-field value of β, and c is an empirical constant. In order to provide the best model for roughness elements characteristic of natural streams and rivers, which almost always have values of σ/H greater than 1/2, the Gaussian elements are treated separately from the flat plate in the regression. For the Gaussian elements, the values of β' are weighted by the drag coefficient, because the predicted drag forces for steeper-shaped elements are more sensitive to the value of β. This gives $\beta_{far} = 0.226$ and $c = 0.353$. For the flat plate, the values of β_{far} and c are determined to be 0.241 and 0.515, respectively. The values for β_{far} for the Gaussian elements and the flat plate are not substantially different from the value of 0.18 determined by *Schlichting* [1979]. By changing the value of β for close spacings, the model is essentially accounting for near-field effects through a change in the eddy viscosity of the wake. A lower value of β means that the velocity deficit of the wake does not diffuse as fast in the near field.

[31] Comparisons of the measured and calculated forces and velocities using (17) are given in Figures 7–9. Those for the forces are shown in Figures 7 and 9a. In general, the calculated drag forces for the elements are in reasonable agreement with the measured forces. Forces calculated

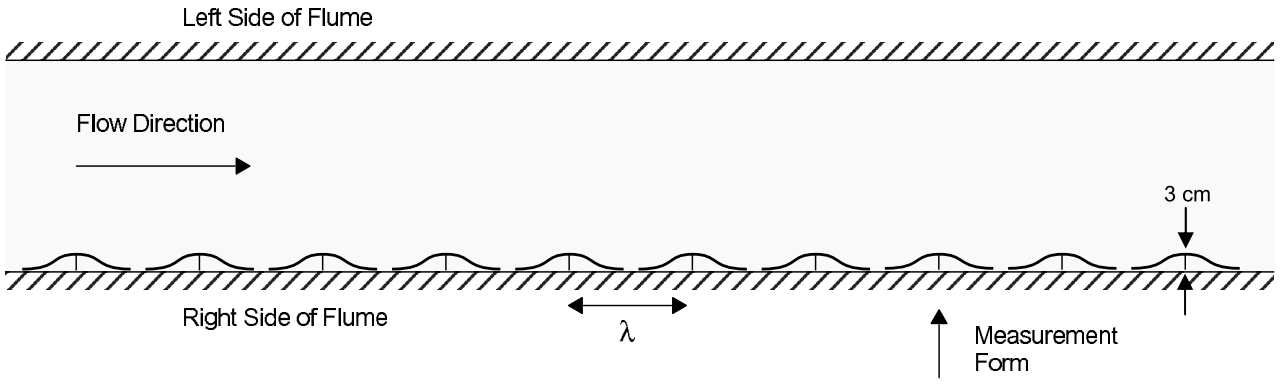

Figure 5. Plan view of the series of 10 regularly spaced roughness elements in the *Hopson* [1999] experiment.

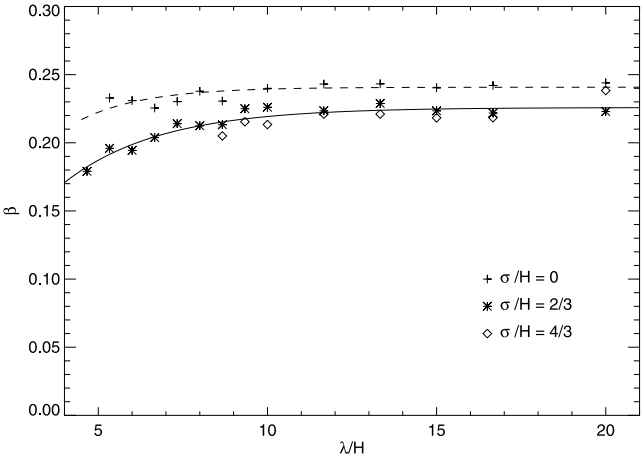

Figure 6. Back-calculated values of the empirical wake constant, β, needed to have perfect agreement between the measured and predicted forces. The solid line is the fit to the data for the Gaussian-shaped elements given by (17). The dashed line is the fit to the data for the flat plate given by (17). For reference, β in the wake of a cylinder in uniform flow has been measured to be 0.18 [*Schlichting*, 1979].

using a constant β that is equal to β_{far} for the flat plate and Gaussian elements are also shown for comparison. Using a constant β results in a difference between the measured and calculated forces that is within 20% for all spacings of the Gaussian elements. A comparison of the measured and calculated velocity profiles for the minimum, maximum, and an intermediate spacings of the elements is shown in Figures 8 and 9b. In general, there is reasonable agreement between the measurements and the calculated outer profile. The greatest deviation is for the closest spacing of the broadest form. This discrepancy may be because the measured spatially averaged velocity for the broadest form was defined by fewer measurements in the streamwise direction than for the other Gaussian form. Figure 8 also shows the dependence of the wake profile on λ and C_D. As the spacing increases the growth in the wake is matched by a decrease in the velocity deficit. For a given spacing, an increase in the drag coefficient causes an increase in the wake height and the velocity deficit. The match in slope between the wake and calculated outer velocity profile is better for larger velocity deficits.

6. Implications for Velocity and Boundary Shear Stress

[32] The effects of drag on small-scale bank topographic features on the velocity and boundary shear stress fields are demonstrated using a channel based on the geometry and roughness characteristics of a reach near USGS streamflow gauging station, 12323840, Lost Creek near Anaconda, MT. The gravel bedded channel is very narrow and has rough banks as shown in Figure 1a. Quantifying the flow resistance of the banks and including the effects of the banks on the boundary shear stress field is essential for making accurate calculations of flow and sediment transport in narrow, rough channels such as Lost Creek [see *Kean and Smith*, 2005]. The model in this paper is used to determine the roughness height of the bank ($(z_{oT})_{bank}$) from the characteristic size, shape, and spacing of the bank topographic features of Lost Creek. The value of $(z_{oT})_{bank}$ and an estimate of $(z_{oT})_{bed}$ determined from pebble counts is then used by the model of *Kean and Smith* [2004] to compute the reach-averaged velocity field and boundary shear stress distribution for a bankfull flow. Their model, which is an adaptation of the theoretical model of *Houjou et al.* [1990], includes the effects of lateral stresses on the velocity and boundary shear stress fields.

[33] As shown in Figure 1a, the undulations of the bank surface of Lost Creek can be well approximated by a series of Gaussian shapes. Although the banks of Lost Creek are composed of a spectrum of different sized roughness elements, the irregular surface can be modeled as a regular sequence of identical roughness elements defining a surface that would produce the same spatially averaged flow properties. The characteristic geometry of this regular sequence can be specified in terms of the moments of the statistical distributions of the geometric properties of the measured roughness elements. The conversion of an irregular sequence of Gaussian roughness elements into an equivalent regular sequence is the subject of the companion paper [*Kean and Smith*, 2006]. On the basis of two sets of roughness measurements, which include the one shown in Figure 1a, the characteristic geometry of the Gaussian-shaped bank undulations is H = 18.6 cm, σ = 12.8 cm, and λ = 112 cm. Using equation (16), the drag coefficient of this feature is found to be 1.05. The surface of the undulations is assumed to have a skin friction roughness height equal to 0.0005 m. The skin friction roughness height could have been estimated from an analysis of the deviations of the Gaussian fits to the measured surface, which is described by *Kean and Smith* [2005, 2006]. Using the equations in the Appendix, the total rough-

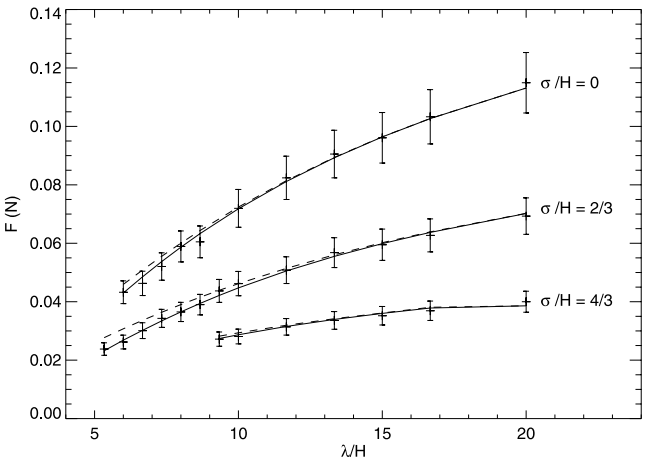

Figure 7. Comparison of measured (dash symbols with error bars) and calculated drag forces (solid and dashed lines). The solid lines are calculated using the expression for β given by (17). The dashed lines are calculated using $\beta = \beta_{far}$, which is 0.226 for the Gaussian elements (σ/H = 2/3 and σ/H = 4/3) and 0.241 for the flat plate (σ/H = 0). The error bars are ±10% of the measured values based on an error analysis of the experimental data.

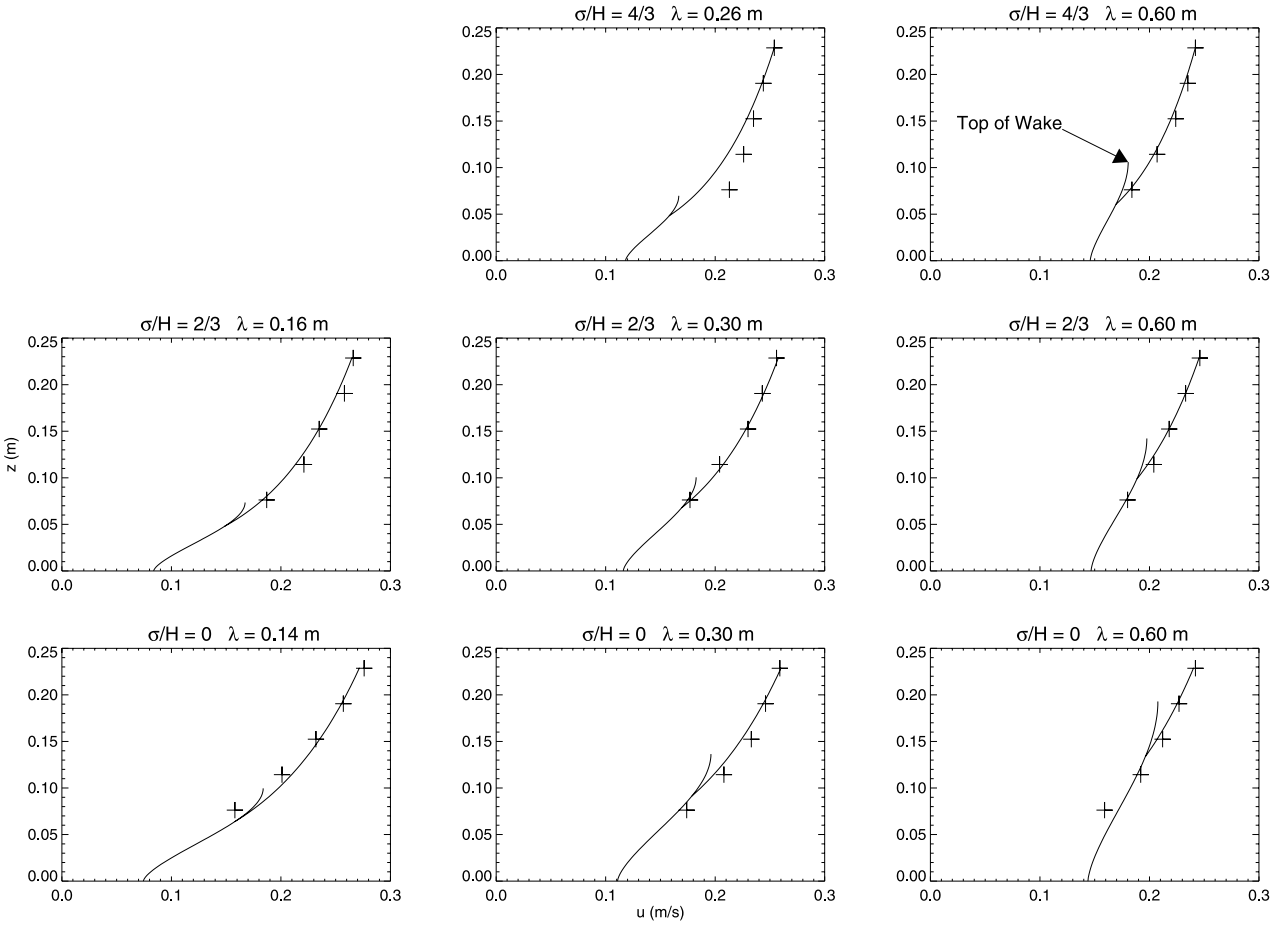

Figure 8. Comparison of measured (symbols) and calculated (line) velocities at wavelengths including the closest and farthest spacings for each of the three element types. The measured velocities are averaged over one wavelength in the streamwise direction, and the calculated profile is made at x = λ, which is the center of the measurement element. The entire wake profile has been drawn to show the top of the wake. The internal boundary layer profile is not shown. The reference velocity used to calculate the drag on the element is found by averaging the calculated velocity profile over the plan view area of element. The limit of this average in the z direction is 0.03 m, the height of the elements.

ness height of the modeled bank is determined to be 0.028 m. The roughness height of the bed is specified from the size distribution of the bed material using the relation $(z_{oT})_{bed} = 0.21D_{84z}$, where D_{84z} is diameter of the 84th percentile of the size distribution of the vertically oriented axis [*Wiberg and Smith*, 1991]. The value of D_{84z} determined from an aggregate of two Wolman pebble counts [*Wolman*, 1954] was 3.8 cm. The cross section used in the computation is based on an average of 49 cross sections, spaced approximately 1 m apart, and surveyed on 10 November 2004.

[34] Figure 10 shows calculated distributions of reach-averaged velocity and boundary shear stress for a bankfull flow (case 1). For comparison, total boundary shear stress distributions also are shown for (case 2) a calculation having the same bank roughness height as the bed ($(z_{oT})_{bank} = (z_{oT})_{bed} = 0.008$), and (case 3) a calculation that has equal bed and bank roughness but does not include the effects of lateral stress on the velocity and boundary shear stress. In the later case, the boundary shear stress is given by the local depth-slope product, and the velocity field is defined by vertical profiles based on the two-part eddy viscosity of *Rattray and Mitsuda* [1974] (see *Wiberg and Smith* [1991]). Figure 10b shows that the additional flow resistance created by drag on the topographic features has a substantial effect on the distribution of stress in the channel. More fluid stress is transmitted to the rough banks, which, in turn, reduces the near-bank bed stress relative to what it would be if the banks were smoother or if lateral stresses were neglected.

[35] A summary of the flow and roughness properties for all three cases is listed in Table 2. Table 2 shows that the flow resistance created by the bank topographic features causes an 18% reduction in discharge from the case with equal bed and bank roughness. Neglecting both the drag on the topographic bank features and the effects of lateral stresses results channel results in a 56% overestimate in discharge. Table 2 also contains back-calculated values of the Manning coefficient for each case. A description of another application of the methods described in this paper to the data from the two other streams presented in Figure 1

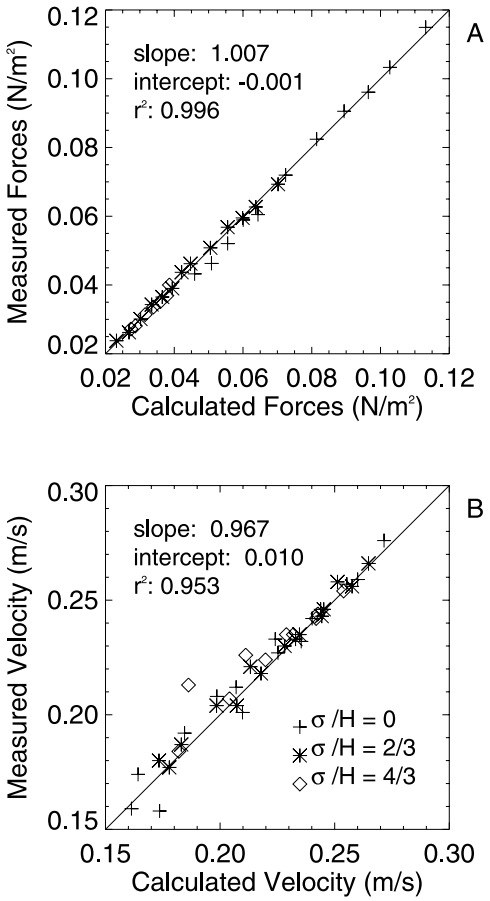

Figure 9. Scatter plot comparisons of (a) calculated and measured forces and (b) calculated and measured velocities for the data shown in Figures 7 and 8. The solid line is the line of perfect agreement. The slope, intercept, and r^2 of the line of best fit (not shown) through all of the data are listed in the top of each plot.

(Rock Creek and Whitewater River) is given by *Kean and Smith* [2005].

7. Summary and Conclusions

[36] This paper demonstrates that including the effects of drag on natural topographic features is essential for determining the flow and boundary shear stress fields near boundaries with small-scale roughness. This can be done by explicitly calculating the drag on the features using its drag coefficient and an appropriate reference velocity that includes the wake of the upstream feature. Field measurements of surface topography showed that the shape of a wide variety of natural topographic bank features can be approximated suitably by a Gaussian curve. The drag coefficients of these shapes can be estimated from the laboratory measurements of *Hopson* [1999]. A simple model for flow over a regular sequence of topographic features is validated in this paper using the *Hopson* [1999] measurements. The experimental data set also was used to determine the constant that scales the eddy viscosity in the wake of the Gaussian features. Using this constant, the model is in good agreement with the measurements of the widely spaced features and is within 20% for the close spacings. The approach is successful because it identifies the appropriate turbulent length scales of the flow regions used to determine the reference velocity. An empirical adjustment is developed to account for the nonlinearities in the near-field wake and improve the agreement for closely spaced features.

[37] The effects of topographic features on reach-averaged patterns of velocity and boundary shear stress can be determined by combining the methods described in this paper with a flow model such as that of *Kean and Smith* [2004]. Application of such an approach to a channel based on that of Lost Creek, near Anaconda, MT, demonstrates that drag on topographic bank features substantially reduces the near-bank velocity and boundary shear stress. In narrow channels the influence of the bank extends to the center of the channel.

[38] The methods presented in this paper provide a foundation for determining the near-bank flow and boundary shear stress fields that control lateral erosion in natural channels, as well as making accurate predictions of stage-discharge relations. Owing to the fact that drag on a feature is primarily controlled by the wake of the feature upstream, a generalization of the model presented in this paper is needed to address the flow effects of irregularity in the size,

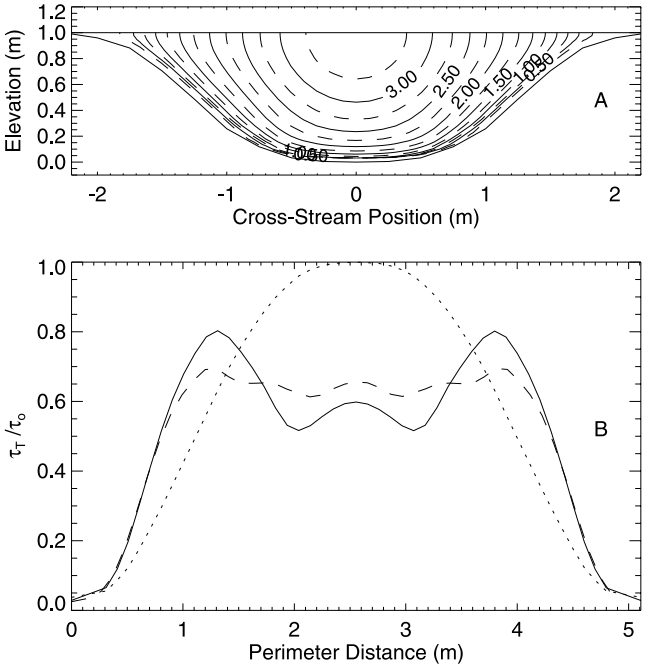

Figure 10. Calculated reach-averaged (a) velocity and (b) boundary shear stress distributions for a channel modeled after Lost Creek near Anaconda, Montana. The cross section in Figure 10a is drawn without any vertical exaggeration. The stress profiles have been normalized by the depth-slope product in the center of the channel, $\tau_o = \rho g h_o S = 147$ N/m^2. Also shown is the boundary shear stress distribution for the case with $(z_o)_{bank} = (z_o)_{bed} = 0.008$ m (dashed line) and the stress profile given by the local depth-slope product (dotted line).

Table 2. Roughness and Flow Parameters for Lost Creek Bankfull Calculations[a]

Case	Lateral Stress	$(z_{oT})_{bed}$, m	$(z_{oT})_{bank}$, m	$(\tau_T/\tau_o)_{center}$	Q, m^3/s	Manning n
1	yes	0.008	0.028	0.60	5.26	0.037
2	yes	0.008	0.008	0.66	6.38	0.030
3	no	0.008	0.008	1.00	8.18	0.024

[a]Depth = 1 m, slope = 0.015, area = 2.53 m^2, and wetted perimeter = 5.11 m.

shape, and spacing of roughness elements. This subject is the focus of our companion paper [*Kean and Smith*, 2006].

Appendix A: Roughness Height for a Regular Sequence of Topographic Elements

[39] The roughness height for a regular sequence of topographic features can be determined from the geometric properties of the features. This is done by first expressing the reference velocity, u_{ref}, as fraction of the velocity at the top of the wake, u_b:

$$u_{ref} = \alpha_2 u_b \tag{A1}$$

where

$$\alpha_2 = \frac{1}{A_{IBL}} \int\limits_{A_{IBL}} \frac{\alpha_1}{\kappa} \ln\left(\frac{z}{z_{oSF}}\right) dA_{IBL} + \frac{1}{A_{wake}} \int\limits_{A_{wake}} \left[1 - g(x) f\left(\frac{z}{b}\right)\right] dA_{wake} \tag{A2}$$

and A_{IBL} is the plan view area of the element within the internal boundary layer, and A_{wake} is the plan view area within the wake. The coefficient α_2 does not contain any flow-related parameters. Substituting (A1) into (15) and dividing the result by τ_{SF} gives

$$\frac{\tau_T}{\tau_{SF}} = 1 + \frac{1}{2} C_D \frac{H}{\lambda} \left(\frac{\alpha_2}{\alpha_0 \alpha_1}\right)^2 \tag{A3}$$

The square root of (A3) gives the ratio between the shear velocities of the outer flow and the internal boundary layer, (u_{*T}/u_{*SF}), and substituting $u_{*SF} = \alpha_0 \alpha_1 u_b$ into that expression yields an expression for (u_{*T}/u_b) that is in terms of known geometric parameters:

$$\frac{u_{*T}}{u_b} = \alpha_0 \alpha_1 \left[1 + \frac{1}{2} C_D \frac{H}{\lambda} \left(\frac{\alpha_2}{\alpha_0 \alpha_1}\right)^2\right]^{1/2} \tag{A4}$$

[40] This expression can be substituted into the velocity matching condition (11) between the wake and the outer profile to give an alternative expression to (12) for the matching height, z_m. Imposing the shear matching condition leads to a different sixth-order polynomial expression for z_m. As a result of employing (A4), the coefficients of this polynomial do not depend on the z_{oT}. Taking the physically meaningful root of this polynomial leads to an expression for the matching height, which is

$$z_m = \frac{b(x_c)}{2^{1/3}} \left[1 + \sqrt{1 - 4\left(\frac{u_{*T}}{u_b}\right) \Big/ \left(3\kappa g(x_c)\right)}\right]^{2/3} \tag{A5}$$

Having determined (u_{*T}/u_b) and z_m, the matching condition (11) can be used to obtain an expression for the roughness height for a regular sequence of elements in terms of known parameters:

$$z_{oT} = z_m \exp\left\{-\kappa \left(\frac{u_{*T}}{u_b}\right)^{-1} \left[1 - g(x_c) f\left(\frac{z_m}{b}\right)\right]\right\} \tag{A6}$$

Notation

A	plan view area of element.
A_{IBL}	plan view area of element within internal boundary layer.
A_{wake}	plan view area of element within wake.
A_1, A_2	constants in wake solution.
B	length of element along axis perpendicular to x and z coordinates.
C_D	drag coefficient of an individual element.
D_{84z}	diameter of 84th percentile of size distribution for vertical axis of bed material.
F	drag force on an individual element.
Fr	Froude number.
H	protrusion height of element.
Q	discharge.
R	reattachment point.
S	water surface slope.
a_1,a_2,a_3	coefficients in equation for z_m.
$b(x)$	wake thickness.
c	empirical constant.
$f(x)$	vertical structure function in wake solution.
$g(x)$	horizontal structure function in wake solution.
h_o	depth in center of channel.
n	Manning coefficient.
u	velocity in downstream direction.
u_b	velocity at top of wake.
u_δ	velocity at top of internal boundary layer.
u_{*IBL}	shear velocity inside internal boundary layer.
u_{*SF}	shear velocity acting on surface of element.
u_{ref}	reference velocity.
x	downstream coordinate.
x_c	x position of crest of element.
x_{dn}	x position of downstream end of element.
x_o	virtual origin.
x_{up}	x position of upstream end of element.
x'	distance downstream from beginning of internal boundary layer.
z	distance away from reference level of elements.
z_m	matching level between wake and outer flow region.
z_{oSF}	roughness height due to skin friction.
z_{oT}	roughness height due to skin friction plus form drag.

$(z_{oT})_{bank}$ bank roughness height due to skin friction plus form drag.
$(z_{oT})_{bed}$ bed roughness height due to skin friction plus form drag.
$\langle\ \rangle$ average of variable over unit cell.
α_0 ratio $u_{*SF}/\langle u_{*IBL}\rangle$.
α_1 ratio $\langle u_{*IBL}\rangle/u_b$.
α_2 ratio u_{ref}/u_b.
β empirical constant scaling eddy viscosity in wake.
β_{far} empirically determined far-field value of β.
β' value of β needed by model to have perfect agreement with measurements.
δ height of internal boundary layer.
γ constant in internal boundary layer equation.
η value of the z coordinate at the boundary.
κ von Karman's constant.
λ spacing of elements.
ρ density of water.
σ streamwise length scale of element.
τ_D form drag shear stress.
τ_{IBL} skin friction shear stress present if element where removed from flow.
τ_o depth-slope product shear stress.
τ_{SF} skin friction shear stress on surface of element.
τ_T total shear stress.

[41] **Acknowledgments.** The authors would especially like to thank Tom Hopson for his careful work on the experiment that was used to test the model described in this paper. Peter McCarthy made the detailed survey of channel topography at Lost Creek. David Kinner, Scott Peckham, Jim Pizzuto, and an anonymous reviewer made many helpful suggestions.

References

Griffin, E. R., J. W. Kean, K. R. Vincent, J. D. Smith, and J. M. Friedman (2005), Modeling effects of bank friction and woody bank vegetation on channel flow and boundary shear stress in the Rio Puerco, New Mexico, *J. Geophys. Res.*, *110*, F04023, doi:10.1029/2005JF000322.

Hopson, T. M. (1999), The form drag of large natural vegetation along the banks of open channels, M. S. thesis, 114 pp., Univ. of Colo., Boulder.

Houjou, K., Y. Shimizu, and C. Ishii (1990), Calculation of boundary shear stress in open channel flow, *J. Hydrosci. Hydraul. Eng.*, *8*, 21–37.

Kean, J. W. (1998), A model for form drag on channel banks, M. S. thesis, 56 pp., Univ. of Colo., Boulder.

Kean, J. W., and J. D. Smith (2004), Flow and boundary shear stress in channels with woody bank vegetation, in *Riparian Vegetation and Fluvial Geomorphology, Water Sci. Appl. Ser.,* vol. 8, edited by S. J. Bennett, and A. Simon, pp. 237–252, AGU, Washington, D. C.

Kean, J. W., and J. D. Smith (2005), Generation and verification of theoretical rating curves in the Whitewater River Basin, KS, *J. Geophys. Res.*, *110*, F04012, doi:10.1029/2004JF000250.

Kean, J. W., and J. D. Smith (2006), Form drag in rivers due to small-scale natural topographic features: 2. Irregular sequences, *J. Geophys. Res.*, *111*, F04010, doi:10.1029/2006JF000490.

Lane, S. N., R. J. Hardy, L. Elliot, and D. B. Ingham (2004), Numerical modeling of flow processes over gravelly surfaces using unstructured grids and numerical porosity treatment, *Water Resour. Res.*, *40*, W01302, doi:10.1029/2002WR001934.

Long, C. E., P. L. Wiberg, and A. R. M. Nowell (1993), Evaluation of von Karman's constant from integral flow parameters, *J. Hydraul. Eng.*, *119*, 1182–1190.

McLean, S. R., and J. D. Smith (1986), A model for flow over two-dimensional bed forms, *J. Hydraul. Eng.*, *112*, 300–317.

Miyake, M. (1965), Transformation of the atmospheric boundary layer over inhomogeneous surfaces, M. S. thesis, Dep. of Atmos. Sci., Univ. of Wash., Seattle.

Nelson, J. M., and J. D. Smith (1989), Mechanics of flow over ripples and dunes, *J. Geophys. Res.*, *94*, 8146–8162.

Nicholas, A. P. (2005), Roughness parameterization in CFD modelling of gravel-bed rivers, in *Computational Fluid Dynamics: Applications in Environmental Hydraulics*, edited by P. D. Bates, S. N. Lane, and R. I. Ferguson, pp. 329–355, John Wiley, Hoboken, N. J.

Olsen, N. R. B., and S. Stokseth (1995), Three-dimensional numerical modelling of water flow in a river with large bed roughness, *J. Hydraul. Res.*, *33*, 571–581.

Patel, V. C. (1998), Perspective: Flow at high Reynolds number and over rough surfaces—Achilles heel of CFD, *J. Fluids Eng.*, *120*, 435–444.

Patel, V. C., and J. Y. Yoon (1995), Application of turbulence models to separated flow over rough surfaces, *J. Fluids Eng.*, *117*, 234–241.

Rattray, M., Jr., and E. Mitsuda (1974), Theoretical analysis of conditions in a salt wedge, *Estuarine Costal Mar. Sci.*, *2*, 373–394.

Schlichting, H. (1979), *Boundary-Layer Theory*, 817 pp., McGraw-Hill, New York.

Schlichting, H., and K. Gersten (2000), *Boundary-Layer Theory,* 8th revised and enlarged ed., 799 pp., Springer, New York.

Smith, J. D., and S. R. McLean (1977), Spatially averaged flow over a wavy surface, *J. Geophys. Res.*, *82*, 1735–1746.

Walmsley, J. L. (1989), Internal boundary-layer height formulae—A comparison with atmospheric data, *Boundary Layer Meteorol.*, *47*, 251–262.

Wiberg, P. L., and J. D. Smith (1991), Velocity distribution and bed roughness in high-gradient streams, *Water Resour. Res.*, *27*(5), 825–838.

Wolman, M. G. (1954), A method of sampling coarse river-bed material, *Eos Trans. AGU*, *35*(6), 951–956.

J. W. Kean and J. D. Smith, U.S. Geological Survey, 3215 Marine Street, E-127, Boulder, CO 80303, USA. (jwkean@usgs.gov)